Peak-Seeking Optimization of Spanwise Lift Distribution for Wings in Formation Flight

Curt Hanson[1] and John J. Ryan[2]
NASA Dryden Flight Research Center, Edwards, California, 93523

      A method is presented for the in-flight optimization of the lift distribution across the wing for minimum drag of an aircraft in formation flight. The usual elliptical distribution that is optimal for a given wing with a given span is no longer optimal for the trailing wing in a formation due to the asymmetric nature of the encountered flow field. Control surfaces along the trailing edge of the wing can be configured to obtain a non-elliptical profile that is more optimal in terms of minimum combined induced and profile drag. Due to the difficult-to-predict nature of formation flight aerodynamics, a Newton-Raphson peak-seeking controller is used to identify in real time the best aileron and flap deployment scheme for minimum total drag. Simulation results show that the peak-seeking controller correctly identifies an optimal trim configuration that provides additional drag savings above those achieved with conventional anti-symmetric aileron trim.

Nomenclature

Symbols

AR	=	aspect ratio
b	=	wing span, meters
b_J	=	gradient of the cost function approximation, Newtons per degree
C_L	=	total lift coefficient
D_p	=	profile drag, Newtons
D_i	=	total induced drag, Newtons
$\bar{D}_i$	=	local induced drag due to wake downwash, Newtons
g	=	gravitational acceleration, meters per second squared
I	=	identity matrix
H	=	vector of inputs to the cost function approximation
J	=	cost function, Newtons
k_u	=	command gain
$\bar{L}$	=	local lift vector rotated due to wake downwash, Newtons
$\bar{L}'$	=	local lift vector rotated due to wake downwash and vortex upwash, Newtons
m	=	airplane mass, kilograms
m_J	=	curvature of the cost function approximation, Newtons per degree squared
M	=	averaging filter sample length
N	=	number of consecutive measurements used in each iteration of the Kalman filter
P	=	covariance matrix
q	=	system noise
Q	=	variance of the system noise
r_c	=	viscous core radius, meters
r	=	measurement uncertainty
R	=	variance of the measurement uncertainty
s	=	Laplace operator
S	=	wing area, meters squared

---

[1] Aerospace Engineer, Flight Controls and Dynamics Branch, P.O. Box 273/ MS 4840D, AIAA Member.
[2] Aerospace Engineer, Flight Controls and Dynamics Branch, P.O. Box 273/ MS 4840D, AIAA Member.

American Institute of Aeronautics and Astronautics

$\bar{T}_i$	=	local induced thrust due to vortex upwash, Newtons
u	=	control surface command, degrees
u^*	=	optimal split inboard aileron-flap command, degrees
V	=	velocity, meters per second
$\bar{V}$	=	local velocity vector rotated due to wake downwash, meters per second
$\bar{V}'$	=	local velocity vector rotated due to vortex upwash, meters per second
y	=	spanwise coordinate, meters
Δy	=	lateral separation between the wing centerlines, meters
α	=	angle of attack, radians
Γ	=	circulation strength, meters squared per second
δ	=	control surface deflection, degrees
Δ	=	perturbation
ε_1	=	gradient threshold, Newtons per degree
ε_2	=	curvature threshold, Newtons per degree squared
ζ	=	vector of coefficients for the cost function approximation
$\hat{\zeta}$	=	estimated vector of coefficients for the cost function approximation
ρ	=	atmospheric density, kilograms per cubic meter
Φ	=	state transition matrix

Superscripts

$-$	=	previous update
$+$	=	current update
1,1	=	upper left entry
2,2	=	lower right entry
a	=	aileron
f	=	flap
ib	=	inboard
ob	=	outboard

Subscripts

0	=	initial value
k	=	discrete value at the current iteration
$k-1$	=	discrete value at the previous iteration
∞	=	freestream

I. Introduction

For two aircraft flying in formation, there exist certain formation geometries that produce disturbances on the trailing aircraft caused by the wingtip vortices of the leading aircraft. A subset of these geometries allows the trailing aircraft to re-trim at a lower thrust setting due to a reduction in induced drag. Flight experiments have shown that the trailing aircraft is typically able to achieve a substantial 10-20% drag reduction.[1-3]

The vortex upwash is asymmetric across the span of the trailing wing, necessitating roll trim to maintain wings-level flight and thereby desired formation position. Traditional roll trim control scheduling such as anti-symmetric aileron deflection tends to reduce the effectiveness of formation flight. Conversely, unconventional trim schedules can maintain roll trim while simultaneously enhancing the benefits of formation flight. Iglesias[4] showed that larger wing loading near the immersed tip produces a greater reduction in induced drag than an elliptical loading. Hanson[5] analyzed aeroelastic wing twist due to formation flight and reported a greater drag savings for wings with leading-edge up twist near the tips as compared with rigid wings.

The current generation of aircraft does not have the explicit control over the spanwise variations in camber and twist of the wing required to replicate the types of lift distributions reported by Iglesias and Hanson. However, the trim deflections of wing controls such as ailerons, flaps, and spoilers can be optimized to produce a minimum drag solution for a given wing at a specific location and orientation within the upwash field.

A peak-seeking controller has been developed to identify in real time the optimal aileron and flap deflection based upon a measure of total drag, with a quadratic penalty on large surface deflections. Estimates of the gradient and curvature of the cost function are provided by a Kalman filter and used to update the control deflection commands of the immersed wing. The aileron of the opposing wing is used to trim out any residual rolling moment.

The first section of this paper describes the aerodynamics used to model the effects of formation flight. The peak-seeking controller and Kalman filter are then described. Finally, results of the peak-seeking algorithm are presented along with details of the implementation.

II.   Aerodynamic Model

The formation geometry of two wings oriented to reduce drag is shown in Fig. 1. The wings are assumed to be co-planar with at least three wingspans of nose-to-tail separation, which is sufficient longitudinal separation to prevent formation-induced disturbances from acting on the leading wing.[4] A system of spanwise coordinates is referenced to the centerline of the trailing wing. The optimal lateral spacing of the wings aligns the inboard wingtip (i.e., the wingtip closest to the other aircraft) of the trailing wing with the core of the leading wing's trailing vortex.
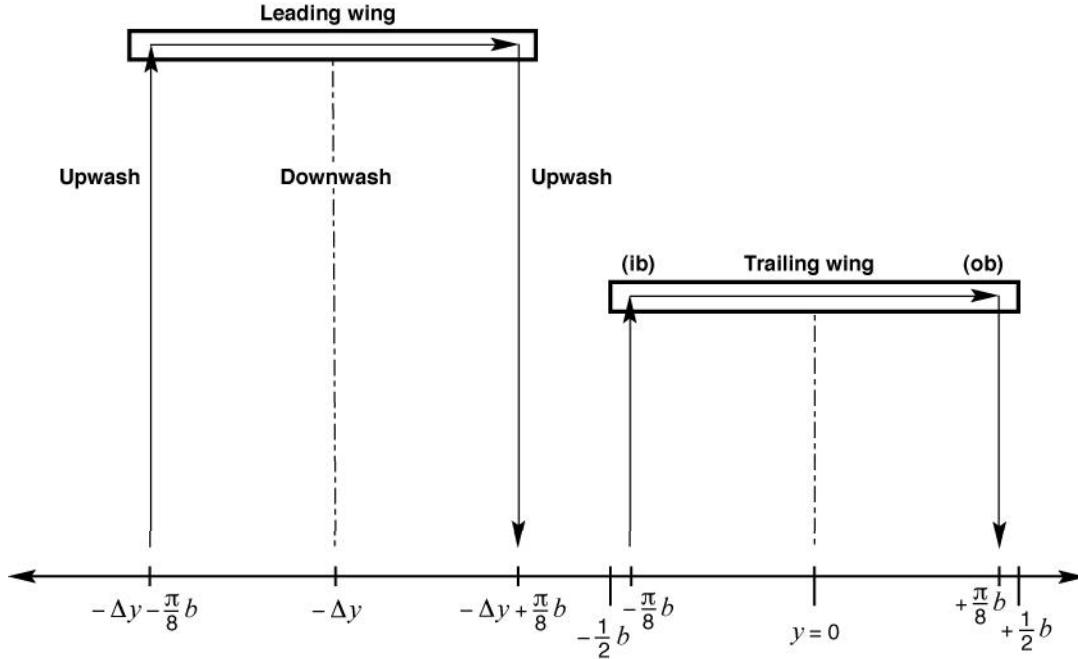

Figure 1. Formation geometry.

Induced drag is caused by downwash behind the wing. The local lift and drag forces acting on an airfoil are by definition perpendicular and parallel, respectively, to the local velocity vector. Downwash immediately behind the wing has the effect of rotating the local lift vector $\bar{L}$ aft, as shown in Fig. 2. The component of the rotated lift vector that is horizontal to the free stream velocity, V_∞ is the local induced drag $\bar{D}_i$. Upwash from the vortex works against the wing's natural downwash, rotating the lift vector $\bar{L}'$ forward to produce an induced thrust $\bar{T}_i$. The net induced drag (or induced thrust) acting on the airfoil is determined by superimposing the wake downwash and vortex upwash to find the final orientation of the local lift vector. The total lift and drag acting on the wing are found by spanwise integration. The untrimmed rolling moment of the wing is similarly found by spanwise integration of the lift vector moment about the longitudinal axis of the aircraft. In this analysis, the upwash-induced side force, yawing moment and pitching moment are ignored, with the justification that they are secondary effects when compared to upwash-induced lift and drag.
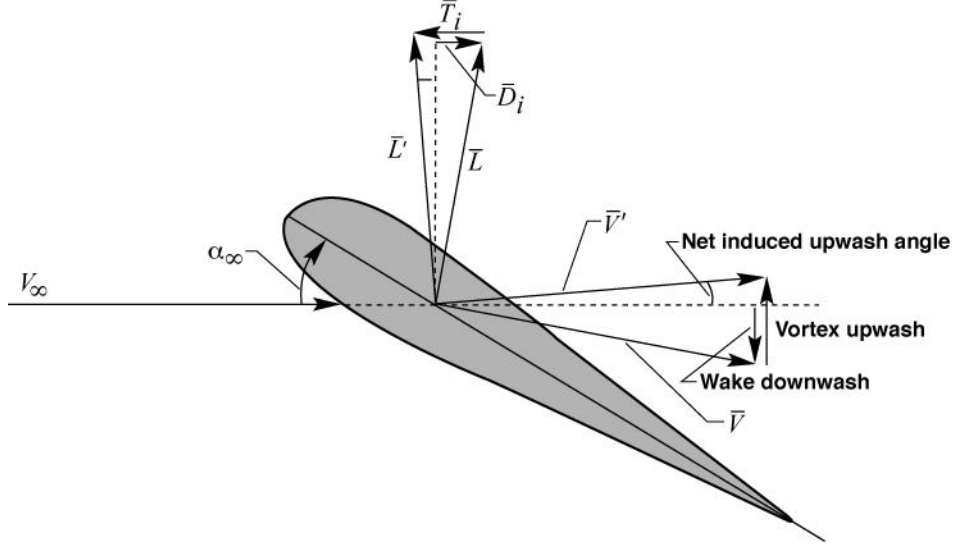
American Institute of Aeronautics and Astronautics

Figure 2. Effects of upwash and downwash on airfoil lift and drag.

A. Calculation of Vortex Upwash

The leading wing is modeled as a horseshoe vortex, consisting of a bound vortex along the wing and semi-infinite trailing vortices streaming from the wingtips. The streaming vortices can be considered as wingtip vortices that have undergone the commonly observed roll-up phenomenon.[6] The circulation, or strength per unit length, of the semi-infinite trailing vortices is assumed to be equal to that of the bound vortex along the wing. For longitudinal separations of three to five wingspans, viscous dissipation of the vortex strength is assumed to be negligible. The circulation Γ is approximated with Eq. (1) by applying the Kutta-Joukowski theorem[7] for a wing in 1-*g* wings-level trimmed flight.

$$\Gamma \rho V b = mg \tag{1}$$

Given a known spanwise separation distance Δy between the wings, the induced angle of attack can be can be calculated at any point y along the trailing wing due to both trailing vortices of the lead wing. Applying the Burnham-Hallock tangential velocity profile for a vortex[8] and small-angle approximation, the induced angle of attack is shown in Eq. (2). The use of a viscous vortex core eliminates singularities at the vortex center (i.e. $y = \pm\Delta y$). The viscous core radius r_c for the fully-rolled up vortices was empirically chosen as 4.75% of the wingspan such that the reduction in induced drag on the trailing wing in formation flight was close to the rule-of-thumb value of 50%.

$$\alpha_i(y) = \frac{\Gamma}{2\pi V}\left[\frac{\Delta y - \frac{\pi}{8}b + y}{\left(\Delta y - \frac{\pi}{8}b + y\right)^2 + r_c^2} - \frac{\Delta y + \frac{\pi}{8}b + y}{\left(\Delta y + \frac{\pi}{8}b + y\right)^2 + r_c^2}\right] \tag{2}$$

American Institute of Aeronautics and Astronautics

B. Calculation of Wake Downwash

The trailing wing is also modeled as a horseshoe vortex. The downwash is computed using Eq. (2) and a viscous core radius r_c set to 14% of the wingspan. This value was arrived at empirically so that the total induced drag of the wing flying solo with no formation effects was approximately equal to that predicted by elliptical wing theory, described by Eq. (3). The larger core size also better represents the wake immediately behind the wing, prior to vortex rollup.

$$D_i \cong \frac{1}{2}\rho V^2 S \left(\frac{C_L^2}{\pi AR} \right) = \frac{(mg)^2}{\frac{1}{2}\rho V^2 \pi b^2} \tag{3}$$

Figure 3 shows the induced upwash and downwash profiles across the trailing wing along with the result of combining them through superposition. Note that, the immersed wingtip near $-b/2$ displays a net positive induced angle of attack, producing a forward rotation of the lift vector and a net induced thrust. Conversely, the induced angle of attack at the opposing wingtip is largely unchanged by the presence of the vortex.
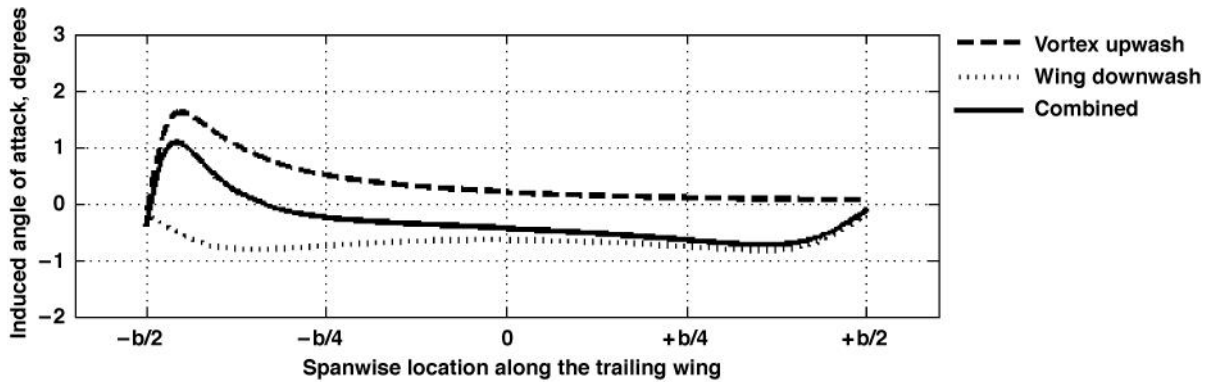

Figure 3. Induced angle of attack for trailing wing in formation.

III. Peak-Seeking Control

The spanwise induced wash angle is shown in Fig. 4, along with a generic straight, tapered wing planform, including locations of ailerons and flaps. Clearly the inboard aileron, closest to the vortex, is in a region of net upwash while the adjacent flap, as well as the control surfaces on the opposing wing half, are all in regions of downwash.

The distribution of lift across the wing can be optimized for minimum drag by adjusting the aileron and flap on the inboard half of the wing to alter the local lift vectors in their vicinity. The immersed aileron is deflected trailing edge down to maximize induced thrust in the region of vortex upwash. The adjacent flap is deflected trailing edge up to counter some of the rolling and root bending moments incurred by the fully-immersed aileron as well as to reduce induced drag. The opposing aileron is deflected as required to maintain roll trim.

The optimal minimum drag configuration of the immersed aileron and flap is difficult to predict due to its dependency on the exact spanwise distribution of the induced angle of attack relative to control surface locations as well as secondary factors such as profile drag due to surface deflection. In some cases it may even be important to consider Mach effects, flow separation, and trim drag due to induced yawing moment. Real-time trim optimization is achieved by a peak-seeking controller based upon a Newton-Raphson algorithm with a Kalman filter to estimate the gradient and curvature of the cost function.[9]

A. Newton-Raphson Command Update

The peak-seeking controller is used to search for the optimal combination of inboard aileron command u^{a-ib} and inboard flap command u^{f-ib}. The measured aileron and flap deflections are denoted as δ^{a-ib} and δ^{f-ib}. These are related via a single parameter δ^{ib} according to the relationship $\delta^{ib} = \frac{1}{2}(\delta^{a-ib} - \delta^{f-ib})$.

American Institute of Aeronautics and Astronautics

Define the cost J to be some function of total drag on the aircraft, which is implicitly a function of the deflection parameter δ^{ib} if all other degrees of freedom in the problem (airspeed, formation spacing) are held constant. The cost function can be approximated using a second-order Taylor series expansion where the gradient b_J and curvature m_J of the function are given by Eqs. (4) and (5).

$$b_J = \frac{\partial J}{\partial \delta^{ib}} \tag{4}$$

$$m_J = \frac{\partial^2 J}{\partial \delta^{ib^2}} \tag{5}$$

The perturbation equation for the cost function is given by Eq. (6), where $\Delta\delta_k^{ib} = \delta_k^{ib} - \delta_{k-1}^{ib}$.

$$\Delta J_k = \Delta\delta_k^{ib} b_J + \frac{1}{2}\left(\Delta\delta_k^{ib}\right)^2 m_J \tag{6}$$

At all local minima and maxima, the first derivative of Eq. (6) with respect to $\Delta\delta_k^{ib}$ is zero. Differentiating, setting equal to zero and solving for δ_k^{ib} yields the Newton-Raphson control command update equation, where the command u^{ib} replaces the deflection δ^{ib}, and the gradient and curvature are estimates. Note that, $u_k^{ib} = \frac{1}{2}\left(u_k^{a-ib} - u_k^{f-ib}\right)$.

$$u_k^{ib} = u_{k-1}^{ib} - \frac{\hat{b}_J}{\hat{m}_J} \tag{7}$$

B. Modeling the Estimation Problem

Clearly from Eq. (7), the convergence of u^{ib} to its optimal value u^* depends upon the accuracy of the estimates of the local gradient $\hat{b}_J$ and curvature $\hat{m}_J$. A Kalman filter is implemented to provide the required estimates. Re-write Eq. (6) as the measurement, or observation, model in Eq. (8).

$$\Delta J_k = H_k \zeta_k + r_k \tag{8}$$

where

$$H_k = \left[\Delta\delta_k^{ib} \quad \frac{1}{2}\left(\Delta\delta_k^{ib}\right)^2\right]$$

$$\zeta_k = \begin{bmatrix} b_J \\ m_J \end{bmatrix}$$

Measurement error is modeled as a zero-mean Gaussian white-noise process r_k that has a variance of R. The system dynamics for this problem are the dynamics of the cost function gradient and curvature due to changes in the control deflection δ^{ib}. Since these dynamics are unknown they are modeled as a random walk, or Brownian, noise process. The system dynamics, or process, model is given by Eq. (9).

$$\zeta_k = \Phi\zeta_{k-1} + q_{k-1} \tag{9}$$

6
American Institute of Aeronautics and Astronautics

The state transition matrix Φ is a 2-by-2 identity matrix. Note that, other than the system noise q_{k-1}, there is no input to Eq. (9) as is often present in the dynamics model of a physical system. The system dynamics noise is modeled as a zero-mean, Gaussian white noise process with a variance of Q.

The Kalman filter is run at a slower rate than the rate at which measurements are available and at which commands are issued to the actuators. N consecutive measurements of the deflection δ^{ib} and associated values of the cost function are stored in the vectors $\{H_k\} \in \mathbb{R}^{N \times 2}$ and $\{J_k\} \in \mathbb{R}^N$, respectively, as shown in Eqs. (10) and (11).

$$\{H_k\} = \begin{bmatrix} \delta_{k,1}^{ib} & \frac{1}{2}\left(\Delta\delta_{k,1}^{ib}\right)^2 \\ \delta_{k,2}^{ib} & \frac{1}{2}\left(\Delta\delta_{k,2}^{ib}\right)^2 \\ \vdots & \vdots \\ \delta_{k,N}^{ib} & \frac{1}{2}\left(\Delta\delta_{k,N}^{ib}\right)^2 \end{bmatrix} \tag{10}$$

$$\{\Delta J_k\} = \begin{bmatrix} \Delta J_{k,1} \\ \Delta J_{k,2} \\ \vdots \\ \Delta J_{k,N} \end{bmatrix} \tag{11}$$

C. Kalman Filter Equations

Because there is no input driving the system's random walk dynamics, the Kalman filter state estimate extrapolation in Eq. (12) is a straightforward replication of the state estimate from the previous frame.

$$\hat{\zeta}_k^- = \Phi\hat{\zeta}_{k-1}^+ \tag{12}$$

The covariance estimate extrapolation is given in Eq. (13).

$$P_k^- = \Phi P_{k-1}^+ \Phi^{\mathrm{T}} + Q \tag{13}$$

The Kalman filter gain $\{K_k\} \in \mathbb{R}^{2 \times N}$ is calculated according to Eq. (14).

$$\{K_k\} = P_k^- \{H_k\}^T [\{H_k\}P_k^- \{H_k\}^T + R]^{-1} \tag{14}$$

The state estimate is updated using Eq. (15).

$$\hat{\zeta}_k^+ = \hat{\zeta}_k^- + \{K_k\}\left[\{\Delta J_k\} - \{H_k\}\hat{\zeta}_k^-\right] \tag{15}$$

The covariance estimate is updated from Eq. (16), where I is an identity matrix of dimension N.

$$P_k^+ = [I - \{K_k\}\{H_k\}]P_k^- \tag{16}$$

American Institute of Aeronautics and Astronautics

The control command is then computed from the Kalman filter estimates as described by Eq. (7). The actual implementation is given by Eq. (17). To avoid unreasonably large commands, the curvature estimate $\hat{\zeta}_{k,2}$ is not used in the calculation if its magnitude is very small, and the magnitude of the slope estimate $\hat{\zeta}_{k,1}$ is limited.

$$u_k = \begin{cases} u_{k-1} - k_u \dfrac{\hat{\zeta}_{k,1}}{\hat{\zeta}_{k,2}}, & \left|\hat{\zeta}_{k,1}\right| < \varepsilon_1, \quad \left|\hat{\zeta}_{k,2}\right| > \varepsilon_2 \\ u_{k-1} - k_u \hat{\zeta}_{k,1}, & \left|\hat{\zeta}_{k,1}\right| < \varepsilon_1, \quad \left|\hat{\zeta}_{k,2}\right| \leq \varepsilon_2 \\ u_{k-1} - k_u \varepsilon_1 sgn(\hat{\zeta}_{k,1}), & \left|\hat{\zeta}_{k,1}\right| \geq \varepsilon_1 \end{cases} \tag{17}$$

IV.   Implementation

The peak-seeking controller was evaluated for a system of two identical aircraft in formation flight with wings having the straight, tapered planform shown in Fig. 4. Kinetic motion of the vehicles was ignored; rather, the two aircraft were held in a fixed position relative to one another corresponding to the location of maximum drag reduction in an anti-symmetric aileron trim configuration. The free stream angle of attack and outboard aileron deflection of the trailing wing were adjusted to maintain constant lift and roll trim,[5] respectively, while the peak-seeking controller commanded split deflection of the immersed aileron-flap combination. The peak seeking controller sought to minimize the cost function in Eq. (18).

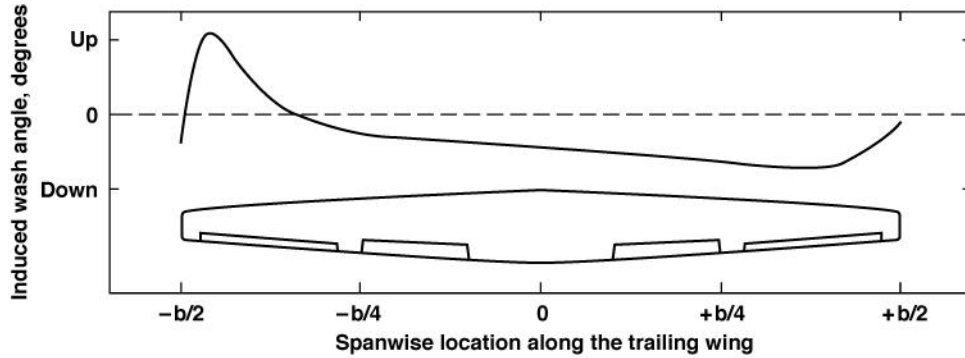$$J = D_p + D_i + \left(D_p^{a-ib} + D_p^{f-ib} + D_p^{a-ob}\right) \tag{18}$$

Figure 4. Spanwise formation effects on wash angle.

The baseline profile drag D_p was assumed to be identical between the two aircraft and fixed independent of the trim angle of attack. D_p was calculated as the lead aircraft's total drag less its induced drag D_i. The induced drag for the trailing aircraft was determined through the spanwise integration of the horizontal components of the rotated local lift vectors across the wing. Finally, the profile drag terms due to surface trim were estimated to be proportional to the square of each control surface deflection, to ensure a convex cost function.

A model of the aileron and flap actuator dynamics was assumed to be the simple first-order transfer function as described by Eq. (19). The relationship between the individual inboard aileron and flap commands is one of equal but opposite magnitude; $u^{a-ib} = -u^{f-ib} = u^{ib}$.

$$\frac{\delta^{ib}}{u^{ib}} = \frac{5}{s+5} \tag{19}$$

American Institute of Aeronautics and Astronautics

To alleviate the effects of measurement noise on commands to the actuators, a simple averaging filter was implemented. Values from M minor frames of the controller were averaged to populate each of the N rows in Eqs. (10) and (11).

A non-linear search routine was used to optimize the tunable parameters of the peak-seeking controller. Table 1 lists the tunable parameters and their values. In addition to these parameters, the search routine was allowed to zero-out the curvature estimate $\hat{\zeta}_{k,2}$ such that the command was only a function of the gradient $\hat{\zeta}_{k,1}$. Due to the extreme sensitivity of the curvature estimate to measurement noise, superior results were consistently achieved by avoiding the use of $\hat{\zeta}_{k,2}$ in the calculation of the command.

Table 1. Peak-seeking controller parameter values.

Parameter	Value
M	3
N	2
R	0.0538
$Q^{1,1}$	0.0007
$Q^{2,2}$	0.0009
$P_0^{1,1}$	0.1456
$P_0^{2,2}$	0.0087
ε_1	41.67
ε_2	0.3629
k_u	0.0005

V.   Results

Truth values of the cost function in Eq. (18) were calculated for values of δ_k^{ib} from -10 (trailing-edge-up) to +10 (trailing-edge-down) in increments of 1/10th of a degree and are plotted in Fig. 5. The inboard aileron and flap deflections were initialized to $\delta_{k=0}^{ib} = -2$ degrees. The corresponding commands were initialized to $u_{k=0}^{ib} = -3$ degrees. This had the effect of initially moving the surfaces in a direction away from the optimal solution.

The peak-seeking controller was run for twenty-five seconds. Normally-distributed random noise with zero mean and a standard deviation of 0.0725 Newtons was applied to the measurements of drag. Similar noise with a standard deviation of 0.2 degrees was applied to the actuator commands. The initial and final inboard aileron command is shown in Fig. 5. The controller achieved the minimum of the cost function, despite its initialization to a deflection of the incorrect sign.
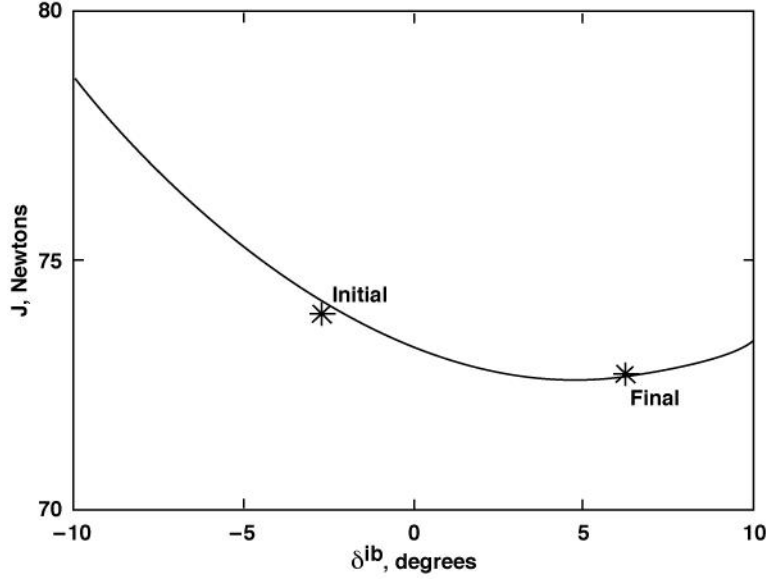
American Institute of Aeronautics and Astronautics

Figure 5. Peak-seeking control solutions.

The peak-seeking aileron deflection of the inboard wing and the opposing aileron's trim deflection are plotted in Fig. 6, along with the cost function value. The initial movement of δ_k^{ib} in the wrong direction is due to the initialization of the command u_k^{ib} to -3 degrees, whereas the position is initialized to -2 degrees. Solutions within a small region of the optimal are achieved within approximately five seconds and maintained for much of the remainder of the simulation. The input and measurement noise produce occasional disturbances in the solution, from which the peak-seeking controller appears to rapidly recover.
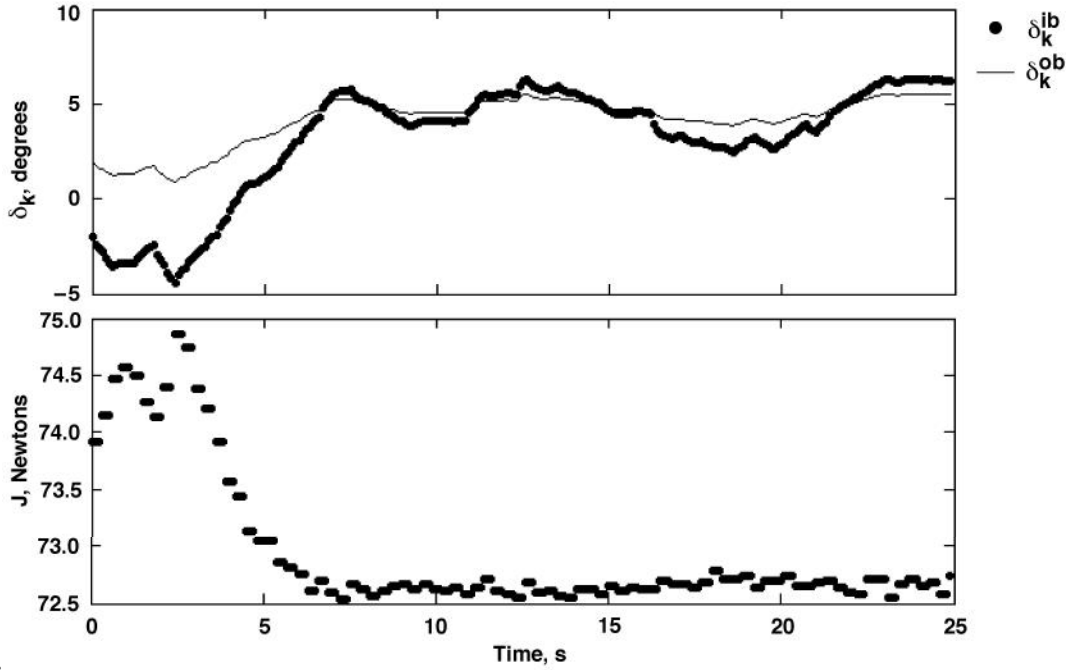

Figure 6. Control deflections and cost function vs. time.

American Institute of Aeronautics and Astronautics

The outboard aileron's trim deflection in Fig. 6 varies significantly less than that of the inboard aileron, indicating that the inboard flap deflection is offsetting much of the rolling moment generated by the inboard aileron. The optimal solution is reached with $\delta^{ib} \cong \delta^{ob} \cong 5$ degrees. This similarity in final values is purely coincidental, a fact confirmed by arbitrarily reducing the control effectiveness of the inboard flap by half to produce a final trim solution in which δ^{ib} and δ^{ob} have distinctly non-similar values.

The percent improvement in total drag due to the non-anti-symmetric trim scheme is plotted in Fig. 7. An additional performance benefit of almost 2% is achieved by the peak-seeking algorithm. It should be noted that the actual drag numbers in this simulation may not accurately predict the results obtainable in flight with aircraft, as the effects of engines, fuselage, empennage, and other non-wing elements have not been modeled. The results do indicate, however, that the peak-seeking algorithm shows promise in identifying the optimal roll trim configuration for a wing in formation flight. An effort is currently underway using high fidelity computational fluid dynamics models to provide more realistic predictions of the potential performance benefits achieved through the optimization of the spanwise lift distribution of a wing in formation flight.
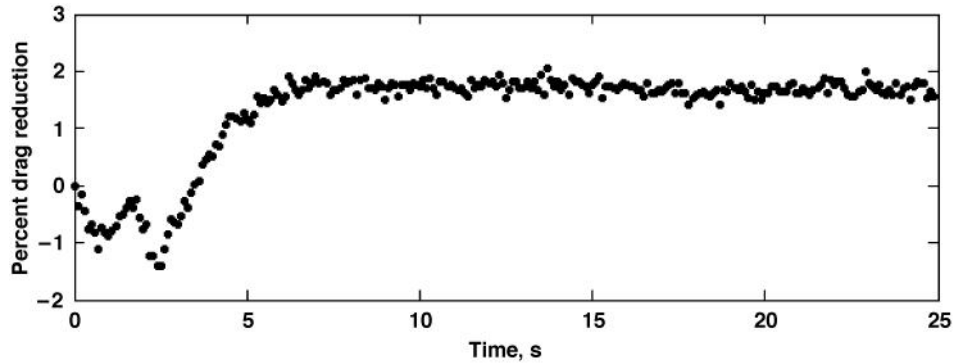

Figure 7. Percent improvement in total drag due to asymmetric trim vs. antisymmetric trim, both in formation flight.

VI.   Summary

A peak-seeking control algorithm has been applied to the optimization of the roll trim for minimum drag of a wing in formation flight. The peak-seeking controller uses a Kalman filter to estimate the gradient and curvature of a cost function that describes the dependency of overall aircraft drag on the deflection of the wing control surfaces. It was shown that, due to the asymmetrical angle-of-attack distribution across a wing in formation flight, the peak-seeking controller can identify non-conventional roll trim strategies that improve the benefits of formation flight over traditional anti-symmetric aileron trim.

Work is ongoing to expand the dimension of the peak-seeking controller to allow independent optimization of the aileron and flap commands. Higher fidelity aerodynamic models are also being developed that will explicitly account for drag penalties due to control surface deflections, improving the appropriateness of the performance cost function.

American Institute of Aeronautics and Astronautics

References

[1]Beukenberg, M., and Hummel, D., "Aerodynamics, Performance and Control of Airplanes in Formation Flight," *Proceedings of the 17th Congress of the International Council of the Aeronautical Sciences,* ICAS-90-5.9.3, September 9-14, 1990, pp. 1777-1794.

[2]Vachon, M. J., Ray, R. J., Walsh, K. R., and Ennix, K., "F/A-18 Aircraft Performance Benefits Measured During the Autonomous Formation Flight Project," AIAA 2002-4491, 2002.

[3]Wagner, Maj. G., Jacques, Lt. Col. D., Blake, W., and Pachter, M., "Flight Test Results of Close Formation Flight for Fuel Savings," AIAA 2002-4490, 2002.

[4]Iglesias, S., "Optimum Spanloads Incorporating Wing Structural Considerations and Formation Flying," M.S. Thesis, Virginia Polytechnic Institute and State University, Blacksburg, Virginia, 2000.

[5]Hanson, C., "Static Aeroelastic Effects of Formation Flight for Slender Unswept Wings," NASA/TM-2009-214649, 2009.

[6]Hallock, J. N. and Eberle, W. R., "Aircraft Wake Vortices: A State-of-the-Art Review of the United States R&D Program," DOT/FAA/RD-77-23, 1977.

[7]Prandtl, L., "Applications of Modern Hydrodynamics to Aeronautics, Part II – Applications," NACA Report 116, 1923, pp. 176.

[8]Burnham, D. C., and Hallock, J. N., "Chicago Monostatic Acoustic Vortex Sensing System, Volume IV: Wake Vortex Decay," DOT/FAA/RD-79-103 IV, 1982.

[9]Ryan, J. J. and Speyer, J. L., "Peak-Seeking Control Using Gradient and Hessian Estimates," Proceedings of the 2010 American Control Conference, Baltimore, Maryland , June 30-July 2, 2010, pp. 611-616.